Iterative Demapping for OFDM with Zero-Padding or Cyclic Prefix

Stephan Pfletschinger
Centre Tecnològic de Telecomunicacions de Catalunya (CTTC)
Gran Capità 2-4, 08034 Barcelona, Spain
Email: stephan.pfletschinger@cttc.es

Frieder Sanzi
Business Unit Logistics
Leuze electronic GmbH & Co KG
In der Braike 1, 73277 Owen/Teck, Germany
Email: friedrich.sanzi@leuze.de

***Abstract*— In this paper, we extend the iterative demapping technique, also known as turbo demodulation, to OFDM. We first introduce an inner code which serves to remove the error floor, which is present in current iterative demapping schemes. This technique is then applied to OFDM with cyclic prefix or zero-padding. Using the EXIT chart, we illustrate the performance differences of various mappings and design a low-complexity inner coding scheme based on differential encoding with code doping. It is shown that this scheme removes the error floor without altering the code rate and while adding very little complexity.**

I. Introduction and System Model

In modern wireless communication systems, the preferred modulation scheme is coded OFDM due to its ability to deal efficiently with multipath fading channels. The increasingly popular standards for WLAN employ convolutional coding with subsequent interleaving and OFDM modulation. The combination of coding, bit interleaving and QAM symbol mapping is known as bit-interleaved coded modulation (BICM) [1] and since OFDM decomposes a broadband frequency-selective channel into parallel flat-fading subchannels, the principles of BICM and its decoding can be applied to OFDM systems as well. A near-optimum method with moderate complexity for the decoding of BICM was first described by ten Brink [2] as *iterative demapping* and later adapted to zero-padded (ZP) and cyclic prefix (CP) OFDM by Muquet et al. [3], who called this principle *turbo demodulation*. This scheme, as illustrated in Fig. 1, is based on the turbo principle, considering the convolutional code as outer code and the QAM symbol mapping as inner "code".

In the following, we will describe the decoding process for this system and enhance the coding scheme with an inner code in order to remove the error floor, which is present in the iterative demapping systems described in [2], [3]. This scheme is then applied to both ZP- and CP-OFDM and its performance is evaluated by simulations.

The transmitter and the receiver for BICM with iterative demapping are depicted in Fig. 1. The binary data source generates a bit sequence $\mathbf{x}_2 = (x_2(1), \ldots, x_2(N))$, with $x_2(k) \in \{-1, +1\}$ of length N, which is encoded by a rate R_2 convolutional encoder and bit-interleaved to yield the sequence $\mathbf{x}_1 = (x_1(1), \ldots, x_1(N/R_2))$. This sequence comprises $K = \frac{N}{R_2 M}$ vectors of length M, where M is the number of bits per QAM symbol: $\mathbf{x}_1 = (\mathbf{x}(1), \ldots, \mathbf{x}(K))$ with $\mathbf{x}(k) = (x_1(k), \ldots, x_M(k))^{\mathrm{T}}$. The vectors $\mathbf{x}(k)$ are then mapped to the complex-valued symbols $y_1(k) = \mathrm{map}(\mathbf{x}_1(k))$ of energy $E_\mathrm{S} = R_2 M E_\mathrm{b}$. The transmitted symbol $y_1(k)$ is attenuated by the fading coefficient $h(k)$ and corrupted by complex AWGN with noise variance per component $\sigma_n^2 = N_0/2$. The receiver picks up the faded and noise-corrupted symbol sequence $\mathbf{z}$ of length K.

II. Iterative Demapping

Iterative demapping is an application of the turbo principle, where the mapping is seen as the inner "code". In the receiver, extrinsic information is passed from the outer decoder to a soft demapper, which calculates *a posteriori probabilities* (APP) on the coded bits $\mathbf{x}_1$. We will use in the following the L-value notation, which is convenient and well established in the literature of iterative decoding. The iterative decoder consists of a soft demapper, to be described in the following, and an APP decoder for the outer code, which is usually implemented with the BCJR algorithm.

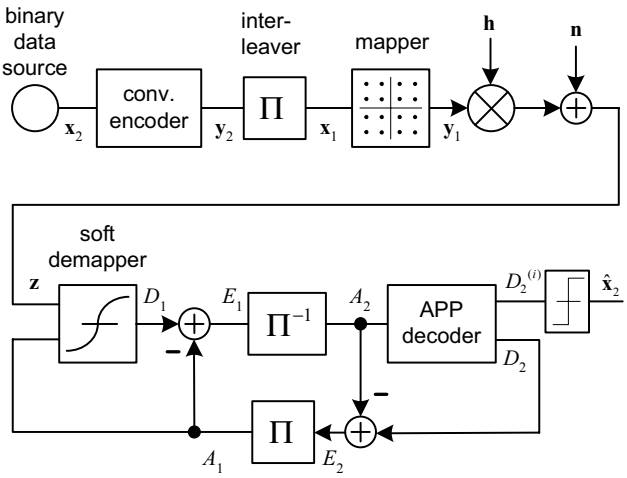

Fig. 1. Transmitter and receiver structure for iterative demapping.

A. Soft Demapping

The APP L-value of $x_m(k)$, which is the output of the soft demapper, is defined as

$$D_{1,m}(k) = \ln \frac{P\left[x_m(k) = +1 \,|\, z(k)\right]}{P\left[x_m(k) = -1 \,|\, z(k)\right]}$$

In the following, we drop the time index k. By defining the sets $\mathcal{X}_{m,\pm 1} = \{\mathbf{x} \,|x_m = \pm 1\}$, applying Bayes' theorem, and assuming that the bits $x_1, \ldots, x_M$ are independent, which is assured by the preceding interleaver, we can write

$$D_{1,m} = A_{1,m} + \ln \frac{\sum_{\hat{\mathbf{x}} \in \mathcal{X}_{m,+1}} p(z|\hat{\mathbf{x}}) P\left[\hat{\mathbf{x}}_{[m]}\right]}{\sum_{\hat{\mathbf{x}} \in \mathcal{X}_{m,-1}} p(z|\hat{\mathbf{x}}) P\left[\hat{\mathbf{x}}_{[m]}\right]} \qquad (1)$$

where $\mathbf{x}_{[m]}$ stands for the vector $\mathbf{x}$ without the element x_m and $A_{1,m} = \ln\left(P[x_m = +1]/P[x_m = -1]\right)$ is the a priori L-value of bit x_m. After some simple calculations [4], we get

$$D_{1,m} = A_{1,m} + \ln \frac{\sum_{\hat{\mathbf{x}} \in \mathcal{X}_{m,+1}} p(z|\hat{\mathbf{x}}) \exp\left(\frac{1}{2}\hat{\mathbf{x}}_{[m]}^{\mathrm{T}} \mathbf{A}_{1[m]}\right)}{\sum_{\hat{\mathbf{x}} \in \mathcal{X}_{m,-1}} p(z|\hat{\mathbf{x}}) \exp\left(\frac{1}{2}\hat{\mathbf{x}}_{[m]}^{\mathrm{T}} \mathbf{A}_{1[m]}\right)}$$

where $\mathbf{A}_1 = (A_{1,1}, \ldots, A_{1,M})^{\mathrm{T}}$. For the Rayleigh fading channel with AWGN, the conditional probability is given by

$$p\left(z|\hat{\mathbf{x}}\right) = p(z|\hat{y}_1) = \frac{1}{2\pi\sigma_n^2} \exp\left(-\frac{|z - h \cdot \hat{y}_1|^2}{2\sigma_n^2}\right)$$

where $\hat{y}_1 = \text{map}(\hat{\mathbf{x}})$. Hence the APP L-value can be written as

$$D_{1,m} = A_{1,m} + \ln \frac{\sum_{\hat{\mathbf{x}} \in \mathcal{X}_{m,+1}} \exp\left(\gamma\left(\hat{\mathbf{x}}\right)\right)}{\sum_{\hat{\mathbf{x}} \in \mathcal{X}_{m,-1}} \exp\left(\gamma\left(\hat{\mathbf{x}}\right)\right)}$$

where the branch metric $\gamma\left(\hat{\mathbf{x}}\right)$ is defined as

$$\gamma\left(\hat{\mathbf{x}}\right) = -\frac{|z - h\hat{y}_1|^2}{2\sigma_n^2} + \frac{1}{2}\hat{\mathbf{x}}_{[m]}^{\mathrm{T}} \mathbf{A}_{1[m]} \qquad (2)$$

B. EXIT Chart Description

Iterative decoding schemes can be analyzed conveniently with the EXIT chart [4], [5]. Fig. 2 shows the EXIT chart for an outer memory 2 convolutional code and various 16-QAM mappings for $E_\mathrm{b}/N_0 = 6$ dB. As is well-known, in iterative decoding, the otherwise optimum Gray mapping performs worst. The EXIT chart provides an excellent tool to choose the mapping and the coding that perform best together. The characteristics of the inner mapping and the outer code should match in such a way that the tunnel in-between is as wide as possible and the intersection is at high values of I_{E1}. The pair of curves which has its intersection closest to $(1, 1)$ yields the lowest remaining BER.

In Fig. 2, the mapping that reaches the highest value of I_{E1} for $I_{A1} = 1$ is the "Bo1" mapping, which was found by Boronka [6] by extensive search. The illustrated mappings are defined as follows (read from bottom left to top right in the constellation diagram):

$$\mathcal{M}_{\text{set part.}} = \{2,7,6,3,5,0,1,4,14,11,10,15,9,12,13,8\}$$
$$\mathcal{M}_{\text{anti-Gray}} = \{1,12,3,14,10,7,8,5,4,9,6,11,15,2,13,0\}$$
$$\mathcal{M}_{\text{Bo1}} = \{11,2,12,1,7,9,6,15,4,10,3,5,14,13,0,8\}$$
$$\mathcal{M}_{\text{natural}} = \{12,13,14,15,8,9,10,11,4,5,6,7,0,1,2,3\}$$

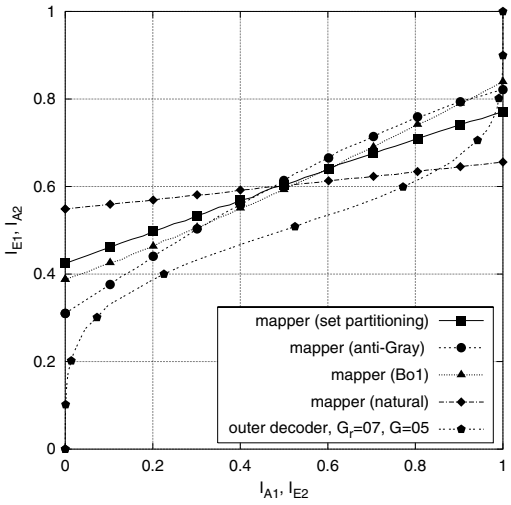

Fig. 2. EXIT chart for outer memory 2 code and various 16-QAM mappings for $E_\mathrm{b}/N_0 = 6$ dB.

For the outer code, a memory 2 code was found to match well with these mappings. Memory 1 codes have transfer curves that tend more to a diagonal line while codes with higher memory tend towards a step function, all curves passing through $(0.5, 0.5)$ [4]. The chosen code is a recursive systematic convolutional (RSC) code with rate $R_2 = 1/2$ and polynomials $G_\mathrm{r} = 07, G = 05$. The corresponding non-recursive code has a nearly identical transfer curve. The transfer curves are plotted for $E_\mathrm{b}/N_0 = 6$ dB. For lower SNRs, the curves are shifted vertically downwards and vice versa. We can see from Fig. 2 that at $E_\mathrm{b}/N_0 = 6$ dB the iterative decoding gets started for all mappings, but will get stuck before reaching the point $(1, 1)$, which indicates an error floor that cannot be overcome by increasing the number of iterations. For higher E_b/N_0, the inner transfer curves will be lifted and the error floor will be lowered, but not eliminated. This behavior can be clearly seen in Fig. 3, where the simulated BER for different numbers of iterations is depicted[1]. The interleaver is pseudo random and of length 128 000 bit for all simulations in this paper. Like in all turbo schemes, the BER performance degrades significantly for short interleaver lengths.

As this error floor behavior is typical for iterative decoding schemes for BICM, we expect that the scheme presented in [3] suffers from the same effect, although not visible in the PER curves presented there. The remaining BER is low enough to be corrected with an additional outer block code with low redundancy, but nevertheless requires some extra effort and lowers the spectral efficiency. In the next section we will discuss a solution which eliminates the error floor without adding redundancy and introduces only very moderate additional complexity.

[1] We found similar results for 64-QAM, where we replaced the Bo1 mapping with a mapping that provides a Hamming distance of 5 bit between each signal point and its next neighbors.

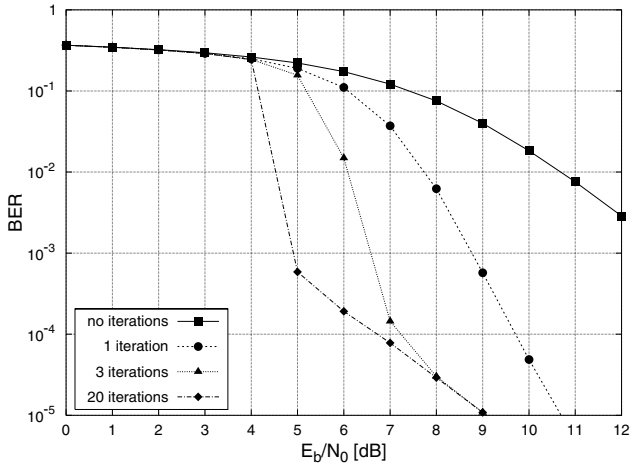

Fig. 3. BER curve for iterative demapping with "Bo 1"-mapping.

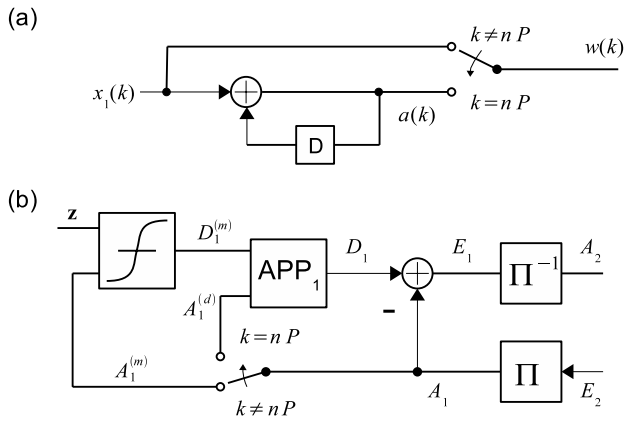

Fig. 4. (a) Code doping of inner recursive rate one convolutional code. (b) Changes in receiver structure to incorporate inner decoder.

C. Code doping

The error floor can be removed if we achieve to "bend up" the inner transfer characteristics in Fig. 2, so that they reach the point $(1, 1)$. A method for achieving this has been described in [7] in a similar context. It consists of introducing a differential encoder between the interleaver and the mapper. This encoder, depicted in Fig. 4 (a), is a rate 1 recursive convolutional code which adds no redundancy and thus has no error correcting capabilities at all. Nevertheless, it introduces dependencies between adjacent bits and thus has a significant influence on the transfer curve, as can be seen in the EXIT chart in Fig. 5. The necessary changes to the receiver structure are illustrated in Fig. 4 (b). The output of the inner differential encoder consists of information bits $(k \neq nP)$ and coded bits $(k = nP)$, $n \in \mathbb{Z}$. In the receiver, the a priori information on the coded bits is thus directed to the APP decoder for the rate 1 code, while a priori information on the information bits is fed to the soft demapper.

The EXIT chart shows that the doping rate P should be chosen rather high in order to bend up the tail of the curve for high I_{A1} without lowering it for small I_{A1}. Also, very small values of P, with $P < M$, would introduce dependencies between mapped bits of the same QAM symbol, contrary to the assumption made for (1). Thus, only few coded bits are injected by the inner encoder. Note that the "systematic doping" described in [4] is the dual approach: there, an inner convolutional encoder is doped with some few information bits and the desired effect is to lift up the inner transfer curve for low I_{A1}. The functioning of the inner code is confirmed by the simulation result in Fig. 6, which compares the BER for iterative demapping with and without inner code.

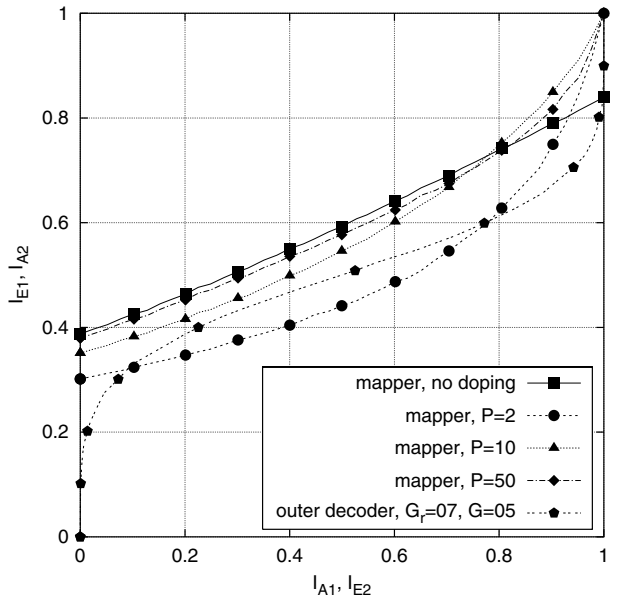

Fig. 5. EXIT chart including inner RSC encoder with code doping and 16-QAM "Bo 1"mapping.

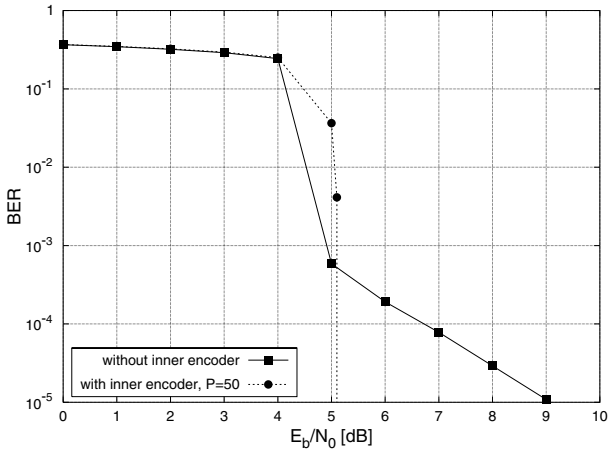

Fig. 6. BER curve for iterative demapping with "Bo 1"mapping with and without inner RSC encoder after 20 iterations. For 10^7 simulated informations bits, no error floor was encountered.

III. Application to OFDM

These ideas can be applied straightforwardly to OFDM as this multicarrier scheme decomposes a frequency-selective channel into N_{C} parallel flat-fading subchannels. We will consider beside the traditional OFDM scheme with cyclic prefix (CP-OFDM) the recently proposed ZP-OFDM, which adds trailing zeros to each OFDM block. In the following, we consider an OFDM system with N_{C} subcarriers and N_{G} guard samples, which are either the cyclically repeated samples of the cyclic prefix or the appended zeros. The total number of samples per OFDM symbol is thus $N_{\mathrm{S}} = N_{\mathrm{C}} + N_{\mathrm{G}}$. The vector $\mathbf{y}_1$ of length N/R_2M is decomposed into $K \triangleq \frac{N}{R_2 M N_{\mathrm{C}}}$ vectors of length N_{C}:

$$\mathbf{y}_1 = \left(\tilde{\mathbf{y}}^{\mathrm{T}}(1), \ldots, \tilde{\mathbf{y}}^{\mathrm{T}}(K)\right)$$

These vectors $\tilde{\mathbf{y}}(k)$ are input to the iFFT transformer as depicted in Fig. 7.

A. Cyclic Prefix OFDM

In CP-OFDM, after the inverse Fourier transform, the last N_{G} samples of each OFDM block are copied and inserted at the beginning of the block. We can thus write the output of the transmitter as

$$\mathbf{s}(k) = \left[\bar{\mathbf{F}}_{\mathrm{cp}}, \mathbf{F}\right]^{\mathcal{H}} \tilde{\mathbf{y}}(k)$$

where $\mathbf{F}$ is the N_{C}-point FFT matrix with entries $F_{\nu,\mu} = \exp(-j2\pi\nu\mu/N_{\mathrm{C}})/\sqrt{N_{\mathrm{C}}}$, $\bar{\mathbf{F}}_{\mathrm{cp}}$ is the $N_{\mathrm{C}} \times N_{\mathrm{G}}$ matrix formed by the last N_{G} columns of $\mathbf{F}$ and $(\cdot)^{\mathcal{H}}$ denotes conjugate transposition. Each block $\mathbf{s}(k)$ is filtered with the impulse response $\mathbf{h} \triangleq [h_0 \cdots h_{N_{\mathrm{G}}}]$ and AWGN $\tilde{\mathbf{n}}(k)$ is added. At the receiver side, after removal of the CP, the received block is Fourier transformed to yield the signal $\mathbf{z}(k)$. It is well known, that this operation diagonalizes the channel (for details see e.g. [8], [9]), resulting in the kth received block

$$\mathbf{z}(k) = \mathrm{diag}\left(\tilde{h}_0 \cdots \tilde{h}_{N_{\mathrm{C}}-1}\right) \tilde{\mathbf{y}}(k) + [\mathbf{0}, \mathbf{F}]\, \tilde{\mathbf{n}}(k)$$

with $\tilde{h}_\mu = \sum_{\nu=0}^{N_c-1} h_\nu \exp(-j2\pi\nu\mu/N_{\mathrm{C}})$ and $\mathbf{0}$ is the $N_{\mathrm{C}} \times N_{\mathrm{G}}$ zero matrix. The noise after the Fourier transform $\mathbf{n}(k) = [\mathbf{0}, \mathbf{F}]\, \tilde{\mathbf{n}}(k)$ is still Gaussian, zero mean and has the same variance σ_n^2. For subchannel μ, this writes simply as $z_\mu = \tilde{h}_\mu \cdot \tilde{y}_\mu + n_\mu$, which allows us to use the metric (2), correspondingly:

$$\gamma_{cp}(\hat{\mathbf{x}}) = -\frac{\left|z_\mu(k) - \tilde{h}_\mu(k)\tilde{y}_\mu(k)\right|^2}{2\sigma_n^2} + \frac{\hat{\mathbf{x}}_{[m]}^{\mathrm{T}} \mathbf{A}_{1[m]}}{2} \quad (3)$$

B. Zero-padded OFDM

OFDM with zero-padding has been proposed recently by Scaglione et al. [10] and has been considered for wireless transmission in [3], [8]. It has been shown that in the noiseless case with ZP-OFDM the transmit symbol can be recovered regardless of the channel zero locations. This is not possible with CP-OFDM where a channel zero at a subcarrier frequency will inevitably destroy that subchannel's symbol. The complete block diagram of ZP-OFDM is depicted in Fig. 7. After inverse

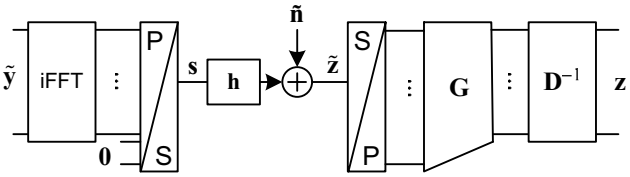

Fig. 7. Block diagram for zero-padded OFDM.

Fourier transformation of the input vector $\tilde{\mathbf{y}}$, N_{G} zeros are appended to the OFDM block, yielding the output signal $\mathbf{s}(k) = \mathbf{F}_{\mathrm{zp}}\tilde{\mathbf{y}}(k) = [\mathbf{F}, \mathbf{0}]^{\mathcal{H}} \tilde{\mathbf{y}}(k)$. The receiver input signal is

$$\begin{aligned}\tilde{\mathbf{z}}(k) &= \mathbf{H}\, \mathbf{F}_{\mathrm{zp}}\, \tilde{\mathbf{y}}(k) + \tilde{\mathbf{n}}(k) \\ &= [\mathbf{H}_0, \mathbf{H}_{\mathrm{zp}}]\, [\mathbf{F}, \mathbf{0}]^{\mathcal{H}}\, \tilde{\mathbf{y}}(k) + \tilde{\mathbf{n}}(k) \\ &= \mathbf{H}_0\, \mathbf{F}^{\mathcal{H}}\, \tilde{\mathbf{y}}(k) + \tilde{\mathbf{n}}(k)\end{aligned}$$

where $\mathbf{H}$ is the $N_{\mathrm{S}} \times N_{\mathrm{S}}$ lower triangular Toeplitz matrix whose first column is $[h_0 \cdots h_{N_{\mathrm{G}}}\ 0 \cdots 0]^{\mathrm{T}}$ and $\mathbf{H} = [\mathbf{H}_0, \mathbf{H}_{\mathrm{zp}}]$ is its partition into the first N_{C} and the last N_{G} columns. $\mathbf{H}_0$ is also Toeplitz and always invertible. In this paper, we will only regard MMSE equalization, but the following procedure can be adapted to other equalizers [3]. Without loss of generality, we assume that the signal variance is unity, i.e. the QAM constellations are normalized to have mean energy $E_{\mathrm{S}} = 1$, then the MMSE equalizer matrix is given by

$$\mathbf{G} = \mathbf{F}\mathbf{H}_0^{\mathcal{H}} \left(N_0 \mathbf{I}_{N_S} + \mathbf{H}_0 \mathbf{H}_0^{\mathcal{H}}\right)^{-1}$$

Thus, the signal after equalization is

$$\mathbf{z}_{\mathrm{G}} = \mathbf{G}\tilde{\mathbf{z}} = \underbrace{\mathbf{G}\mathbf{H}_0\mathbf{F}^{\mathcal{H}}}_{\mathbf{\Delta} = \mathbf{D} + \mathbf{\Delta}_{\mathrm{d}}} \tilde{\mathbf{y}} + \mathbf{G}\tilde{\mathbf{n}}$$

The matrix $\mathbf{D}$ is defined as a diagonal matrix that has the same diagonal as $\mathbf{\Delta}$, $\mathbf{\Delta}_{\mathrm{d}}$ thus contains the deviation of $\mathbf{\Delta}$ from the diagonal form. With this definition, we can write $\mathbf{z}_{\mathrm{G}} = \mathbf{D}\tilde{\mathbf{y}} + \mathbf{\Delta}_{\mathrm{d}}\tilde{\mathbf{y}} + \mathbf{G}\tilde{\mathbf{n}}$. To unbias the equalized signal, it is multiplied with the inverse of the diagonal matrix $\mathbf{D}$:

$$\mathbf{z} = \mathbf{D}^{-1}\mathbf{z}_{\mathrm{G}} = \tilde{\mathbf{y}} + \mathbf{D}^{-1}\left(\mathbf{\Delta}_{\mathrm{d}}\tilde{\mathbf{y}} + \mathbf{G}\tilde{\mathbf{n}}\right)$$

At this point, we see that although white noise is added on the channel, the equalized and unbiased signal is corrupted by colored noise. This noise coloring has to be taken into account in the soft demapper. The covariance matrix of the white noise vector $\tilde{\mathbf{n}}$ is $\mathbf{R}_{\tilde{\mathbf{n}}\tilde{\mathbf{n}}} = E[\tilde{\mathbf{n}}\tilde{\mathbf{n}}^{\mathcal{H}}] = N_0\mathbf{I}_{N_S}$ and thus we can write for the covariance matrix of the noise term $\mathbf{n} = \mathbf{D}^{-1}\left(\mathbf{\Delta}_{\mathrm{d}}\tilde{\mathbf{y}} + \mathbf{G}\tilde{\mathbf{n}}\right)$:

$$\mathbf{R}_{\mathbf{nn}} = E\left[\mathbf{n}\mathbf{n}^{\mathcal{H}}\right] = \mathbf{D}^{-1}\left(\mathbf{\Delta}_{\mathrm{d}}\mathbf{\Delta}_{\mathrm{d}}^{\mathcal{H}} + N_0\mathbf{G}\mathbf{G}^{\mathcal{H}}\right)\mathbf{D}^{-1\mathcal{H}}$$

As in [3] we approximate the covariance matrix by its main diagonal and denote by r_μ the μth element of the main diagonal. The subchannel signal can thus be written as:

$$z_\mu(k) = \tilde{y}_\mu(k) + n_\mu(k)$$

where the noise power of $n_\mu(k)$ is given by $r_\mu(k)$, i.e. it depends on the subcarrier index μ and on the block index k. Although $\tilde{\mathbf{n}}(k)$ is stationary and white, the noise at the output of the equalizer is colored and can change for each block, because the equalizer is recalculated for each block. This leads to the metric

$$\gamma_{zp}\left(\hat{\mathbf{x}}\right) = -\frac{\left|z_\mu(k) - \tilde{y}_\mu(k)\right|^2}{r_\mu(k)} + \frac{\hat{\mathbf{x}}_{[m]}^{\mathrm{T}}\mathbf{A}_{1[m]}}{2} \qquad (4)$$

The extension of the single-carrier iterative demapping like illustrated in Fig. 1 can thus be done by simply adapting the metric increments according to equation (3) and (4), respectively. It is therefore expected that the results of section II carry over to both variants of OFDM.

IV. Simulation Results

Simulations have been carried out with settings according to a WLAN environment, i.e. the number of subcarriers was chosen as $N_\mathrm{C} = 64$ and $N_\mathrm{G} = 16$ guard samples have been inserted. For each OFDM block, a different realization of the channel impulse response $\mathbf{h}$ according to the model A described in [11] has been drawn. As in the examples in section II, the outer code is the RSC code with polynomials $G_\mathrm{r} = 07, G = 05$, which is significantly less complex than the memory 6 code used in the WLAN standards. The interleaver is pseudo random and of length 128 000 bits. The inner code is as described in Fig. 4 and the mapping is 16-QAM "Bo1".

The BER curve for ZP- and CP-OFDM is plotted in Fig. 8, where it is visible that the results of Fig. 6 are directly applicable to ZP-OFDM. We notice a performance gap of slightly less than 1 dB in favour of ZP-OFDM. This difference can be explained by the different energy content of the guard interval: while in the cyclic prefix additional energy is transmitted in the guard interval, the zero-padding adds redundancy but no additional transmit energy to an OFDM block. The energy per information bit is given as $E_\mathrm{b} = \frac{E_S}{R_\mathrm{G} R_2 M}$ for both cases, but the factor R_G differs. While for ZP-OFDM $R_\mathrm{G} = 1$ holds, for CP-OFDM, it holds $R_\mathrm{G} = N_\mathrm{C}/N_\mathrm{S} = 0.8$, which corresponds for the chosen guard interval to -0.97 dB. Thus for the same E_b/N_0-value, the noise is by $10\lg N_\mathrm{S}/N_\mathrm{C}$ dB smaller for ZP-OFDM, which fully explains the performance gap.

We have performed simulations with smaller interleaver lengths, which produced no surprising results: the turbo-cliff becomes less pronounced, i.e. the BER curve descends more slowly while the gap between both curves maintains the same.

In light of these results, one might ask: What about the unique ability of ZP-OFDM to recover the transmit symbol regardless of the channel zero locations? We have to keep in mind, that this advantage of ZP-OFDM holds for the noiseless case only, whereas in Fig. 8 we are considering very noisy signals that are additionally encoded with a rate $1/2$ code. Thus, this principal benefit of ZP-OFDM loses ground in this case and the performance difference is due to the smaller transmit energy of ZP-OFDM and depends on the length of the guard interval.

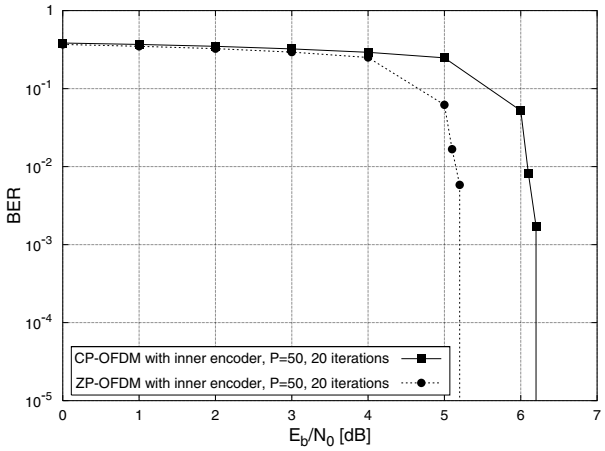

Fig. 8. BER for cyclic-prefix and zero-padded OFDM.

V. Conclusion

We have considered an iterative demapping scheme which is an application of the turbo principle to BICM. As the basic iterative demapping scheme suffers from remaining bit errors, we have introduced an inner differential code which removes the error floor. We have used the EXIT chart and code doping to match the transfer characteristic of the newly introduced inner code to a low-complexity outer convolutional code. This scheme was applied to cyclic prefix and zero-padded OFDM, where in the latter variant the noise color caused by the equalizer was considered in the receiver. Simulations confirmed a performance gap of about $10\lg N_\mathrm{S}/N_\mathrm{C}$ dB in favor of ZP-OFDM.

References

[1] G. Caire, G. Taricco, E. Biglieri, "Bit-interleaved coded modulation," *IEEE Trans. Information Theory,* vol. 44, no. 3, May 1998.

[2] S. ten Brink, J. Speidel, R.H. Yan, "Iterative demapping and decoding for multilevel modulation," *IEEE Globecom '98*, Nov. 1998.

[3] B. Muquet, M. de Courville, P. Duhamel, G.B. Giannakis, P. Magniez, "Turbo demodulation of zero-padded OFDM transmissions," *IEEE Trans. Communications,* vol. 50, no. 11, Nov. 2002.

[4] S. ten Brink, "*Design of Concatenated Coding Schemes based on Iterative Decoding Convergence,*" Ph.D. thesis, University of Stuttgart, 2001, published at Shaker, Aachen, Germany, ISBN 3-8322-0684-1.

[5] S. ten Brink, "Convergence behavior of iteratively decoded parallel concatenated codes," *IEEE Trans. Comm.,* vol. 49, no. 10, Oct. 2001.

[6] A. Boronka, J. Speidel, "A low complexity MIMO system based on BLAST and iterative anti-gray-demapping," *IEEE International Symposium on Personal, Indoor and Mobile Radio Communications (PIMRC),* Sept. 2003.

[7] F. Sanzi, A. Slama, J. Speidel, "Multicarrier code division multiplex with iterative MAP symbol-by-symbol estimation," *IEEE Global Telecommunications Conference (Globecom) '01,* Nov. 2001.

[8] B. Muquet, Z. Wang, G.B. Giannakis, M. de Courville, P. Duhamel, "Cyclic prefixing or zero-padding for wireless multicarrier transmissions?," *IEEE Trans. Communications,* vol. 50, no. 12, Dec. 2002.

[9] Z. Wang, G.B. Giannakis, "Wireless multicarrier communications: where Fourier meets Shannon," *IEEE Signal Processing Mag.*, May 2000.

[10] A. Scaglione, G.B. Giannakis, S. Barbarossa, "Redundant filterbank precoders and equalizers – Part I: Unification and optimal designs, and Part II: Blind channel estimation, synchronization and direct equalization," *IEEE Trans. Signal Processing,* vol 47, no. 7, July 1999.

[11] "Channel models for HIPERLAN/2 in different indoor scenarios," ETSI Normalization Committee, Sophia-Antipolis, France, 1998.